The Characteristics of Self-Resonating Jet Issuing from the Helmholtz Nozzle Combined with a Venturi Tube Structure

M. Yuan[1,2], D. Li[1,2], Y. Kang[1,2], H. Shi[1,2] and Y. Hu[1,2*]

[1] *Hubei Key Laboratory of Waterjet Theory and New Technology, Wuhan University, Wuhan 430072, China*
[2] *School of Power and Mechanical Engineering, Wuhan University, Wuhan 430072, China*

†*Corresponding Author Email: huxiaoyi@whu.edu.cn*

ABSTRACT

Self-resonating waterjet is a new type of waterjet technology that has been widely used for many practical applications. In order to further improve the performance of self-resonating waterjet, the Helmholtz nozzle was improved by replacing the upper part of a traditional contract structure with a venture tube one. This composite nozzle of a venturi tube structure and a Helmholtz resonator was proposed based on the working mechanism of self-resonating waterjet nozzles and the instability of cavitation flow in venturi tubes. Furthermore, the results were also compared with those generated by a conventional Helmholtz nozzle under the same conditions. The frequency of the pressure pulsation in the oscillating cavity and at the outlet was obtained and analyzed by the classical Fast Fourier transform (FFT) method. The results showed that the main frequency of the pressure oscillation rises to 2362.78Hz, and the peak and average values of the pressure are increased by 45% and 12.5% respectively at the outlet of the composite nozzle. In the oscillating cavity of composite nozzle, the pressure oscillations in the central region have higher frequencies and amplitudes, while near the wall are reversed.

NOMENCLATURE

α_v	volume fraction of vapor	R_b	bubble radius
C_s	Smagorinsky coefficient	S_{ij}	average shear rate tensor
C_K	Kolmogorov constant	u	velocity of the mixed phase medium
E	uncertainty of the experiment system	v	molecular viscosity coefficient of the mixed phase medium
E_s	uncertainty of the pressure sensor		
E_l	uncertainty of the data logger	v_τ	Sub-grid viscous viscosity coefficient
p	local far-field pressure		
$\dot{m}^-$	evaporation rate of the water below the saturated vapor pressure	$\overline{\tau}_{ij}$	Subgrid-Scale stress
		ρ	density of the mixed phase medium
$\dot{m}^+$	condensation rate of vapor above the saturated vapor pressure	ρ_v	vapor density
		ρ_l	liquid density
n_b	bubble number density	Δ	filter scale
$\overline{p}$	pressure the mixed phase medium	Ω_{ij}	antisymmetric vorticity tensor
p_v	local saturation vapor pressure		

1. INTRODUCTION

In recent decades, high-speed waterjet technology is rapidly developing in many practical and industrial applications, such as cutting (Hsu *et al.* 2013), mining exploring and developing (Lu *et al.* 2015; Chen *et al.* 2019), processing of materials (Zelenak *et al.* 2015; Annoni *et al.* 2008) and heat transfer (Gould *et al.* 2015). In addition, due to its unique nature of non-thermal effect, high-speed waterjets occupy a special position in machining thermal-sensitive materials (Hu *et al.* 2014). With the development of the modern industry, higher requirements for waterjet technology were put forward. As a result, new types of water jets have emerged in succession, such as cavitating waterjet (Soyama, 2013), abrasive waterjet (Ishfaq *et al.* 2018), and self-resonating waterjet (Liu *et al.* 2018).

As a typical new type of waterjet, they can produce effective pulsed waterjet without using any moving parts in the supply system, and also have the advantages of a cavitating jet (Chahine and Johnson, 1985). The impact damage capability and working efficiency of the self-resonating jet are much greater than the continuous jet under the same pressure. Therefore, the application of self-resonating jet can greatly improve the efficiency among rock breaking, cutting, cleaning and drilling, and has important industrial application value (Li *et al.* 2005). Currently, the most commonly used self-resonating jet nozzles are Helmholtz nozzles and organ-pipe nozzles. The Helmholtz nozzle was put forward by Liao *et al.* (2003), which is based on the self-resonating jet proposed by *Johnson et al.* (1981). The Helmholtz nozzle is mainly composed of upstream nozzle, oscillating cavity, collision wall and downstream nozzle (as shown in Fig 1). The phenomenon of self-resonating oscillation occurs since the unique shape of the nozzle, which causes pressure fluctuations and the increase of pressure peak at the nozzle outlet.

Because of these unique advantages, self-resonating waterjet is thus focused by researchers, especially in the aspects of generation mechanism and optimization of nozzle structure. In more specific terms, in order to further improve the performance of the self-resonating jet, many researchers are committed to understanding the oscillating mechanisms and optimizing Nozzle structure. Morel studied the self-resonating jet induced by the gas jet through the axisymmetric cavity (Helmholtz oscillating cavity) and found that the occurrence of self-resonating oscillation includes three mechanisms, the first is the instability of the jet shear layer and its amplification, the second is the resonance of cavity and the third is the periodic feedback interference of the collision shear layer (Morel & Thomas 1979). Dehkhoda and Hood (2013; 2014)

using self-resonating waterjet to impact different kinds of rocks and found that the pulsation frequency is the key factor for causing internal breakdown in the granite samples. Maganathan *et al.* (2002) used PIV technology to test the unsteady flow in a rectangular cavity under different working conditions. It has been found that small-scale vortex is formed in the upstream of cavity, and then merges to form large-scale vortex ring with evolution in the downstream direction. Kuo *et al.* (2000) studied self-resonating oscillation induced by horizontal cover plate above cavity and found that the main reason of nonlinear variation is the interaction between vortex ring and the collision wall. For another, obvious separation flow was observed at the upstream nozzle, which was verified by Rockwell *et al.* (2003) and Geveci *et al.* (2004) through visual testing and sound pressure measurements.
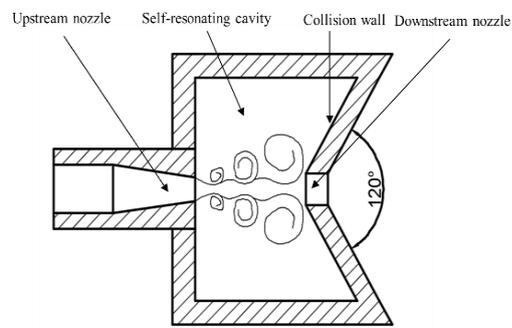

Fig. 1. Schematic diagram of the 120° -impinging edge Helmholtz nozzle.

On the other hand, some researchers are trying to enhance the oscillation performance of self-resonating jet by optimizing the structures of nozzles. Kolsek *et al.* (2007) studied the relationship between nozzle structure parameters and the frequency of oscillation through numerical simulation, and obtained the vortex structure and its evolution process in the cavity. Fang *et al.* (2012) studied the influence of collision wall on self-resonating jet by numerical simulation. The result showed that all of collapse walls will influence the self-resonating waterjet, and the performance of self-resonating jet is optimal when the shape of the collision wall is same.

In general, for Helmholtz nozzles, previous studies have primarily focused on the ratio of upstream nozzle diameter and lower nozzle diameter, the ratio of cavity length and upstream nozzle diameter, the ratio of cavity diameter and upstream nozzle diameter and the shape of collision wall. There is no research aims to explore how the shape of upstream nozzle influence the jet performance at present. Moreover, it is worth noting that the instability of

the shear layer close to the upper stream nozzle is the fundamental cause of oscillation. Partial cavitation is inherently unsteady in nature and causes significant oscillations. The structural characteristics and working principle of the venturi determine that the fluid flowing through the venturi is prone to cavitation (Sato *et al.* 2003). Yazici *et al.* (2007) studied the cavitation flow in the venturi and the results show that cavitation flow has a wide range of vibration frequencies. Chen *et al.* (2015) studied the quasi-periodic pressure pulsations in venturi tubes under cavitation conditions and found that pressure pulsation has a strong connection with the evolution of cavitation clouds. Cloud cavitation is one form of cavitation instability often observed for partial cavitation, in which large sections of the cavity are regularly shed from the main cavity and appear as cloud like structures in the cavity wake (Stutz & Reboud 2000). Others, the geometric size, shape and machining accuracy of the Venturi tube have an important influence on the shear layer, especially in the formation and separation of vortices in the shear layer and the characteristics of the disturbance (Barre *et al.* 2009).

In the present study, aiming at further improving the performance of self-resonating jet for better and more efficient utilizations, self-resonating jet issuing from two structure were studied and contrasted by numerical simulation: the Helmholtz nozzle and the composite nozzle (replacing the upper part of a traditional contract structure with a venture tube one). Moreover, the results of numerical simulations were verified by experiment. The velocity distribution and the evolution progress of the vortex in the cavity are the focus of attention. In addition, the classical Fast Fourier transform (FFT) method was used in filtering and analyzing the characteristics of pressure signals in the cavity. The simulation was conducted using the commercial software package FLUENT 16.0. It took over three months to complete the computational work on a workstation with a total of 40 CPU cores. The present study explores the relationship between the upstream nozzle structure and the self-resonating oscillation frequency, could serve as a supplement for the utilization of self-resonating waterjet in a more efficient way.

2. NUMERICAL FORMULATION

2.1 Numerical Methods

The numerical simulation uses fundamental equations to illuminate the basic characteristics of cavitating flow in the Helmholtz nozzle and the composite nozzle. Large eddy simulation (LES) is an important numerical simulation method developed in the field of computational fluid dynamics in recent

years. It is considered to be one of the most promising turbulent numerical simulation development directions. This article uses the LES method. Main features of mathematical formulations are given below.

2.1.1 Fundamental Equations

In the computational framework based on NS equations, the homogeneous equilibrium flow model (HEM) has prominent advantages, especially in the prediction of cavitation and other multiphase flow problems, showing good calculation stability and applicability. The cavitation model is widely used in the calculation of vapor-liquid two-phase flow, which has been verified in experiments. In the present paper, the cavitation flow was modeled using the single fluid approach by treating the two liquid/vapor phases as a homogenous mixture. Under the above-mentioned homogeneous flow condition assumption, the slip velocity was 0. The homogenous equilibrium flow hypothesis was used in the calculation, and the N-S equation for small-scale pulsation filtering based on Favre averaging is：

$$\frac{\partial \overline{u}_i}{\partial x_i} = 0 \tag{1}$$

$$\frac{\partial \overline{u}_i}{\partial t} + \frac{\partial \overline{u}_i \overline{u}_j}{\partial x_j} = -\frac{1}{\rho}\frac{\partial \overline{p}}{\partial x_i} + \nu \frac{\partial^2 \overline{u}_i}{\partial x_j \partial x_j} - \frac{\partial (\overline{u_i u_j} - \overline{u}_i \overline{u}_j)}{\partial x_j} \tag{2}$$

here ρ, u, $\overline{p}$ are the density, velocity and pressure of the mixed phase medium; ν is the molecular viscosity coefficient of the mixed phase medium;

2.1.2 Subgrid- Scale Stress Model

Germano (1991) and Lilly (1992) developed the dynamic subgrid-Scale stress model (DSM) in order to calculate the Subgrid-Scale stress $\overline{\tau}_{ij}$.

$$\overline{\tau}_{ij} = \left(\overline{u}_i \overline{u}_j - \overline{u_i u_j} \right) = 2\nu_\tau \overline{S}_{ij} - \frac{1}{3}\overline{\tau}_{kk}\delta_{ij} \tag{3}$$

The formula for calculating the Sub-grid viscous viscosity coefficient ν_t and Smagorinsky coefficient C_s is as follows:

$$\nu_\tau = (C_s \Delta)^2 (2\overline{S}_{ij}\overline{S}_{ij})^{1/2} \tag{4}$$

$$C_s = \frac{1}{\pi}(\frac{2}{3C_K})^{3/4} \tag{5}$$

Where: $\overline{S}_{ij}$ is the average shear rate tensor; Δ is the filter scale; C_K is the Kolmogorov constant.

2.1.3 Cavitation Model

Schnerr and Sauer cavitation model is employed to predict cavitating flow, whose convergence is quick and the numerical simulation results are stable (Yuan *et al.* 2001). Empirical coefficients do not exist in the model and it is one relatively ideal cavitation model. The solution of cavitation is achieved by introducing an additional transport-based equation for the vapor phase volume fraction. In the solution process,
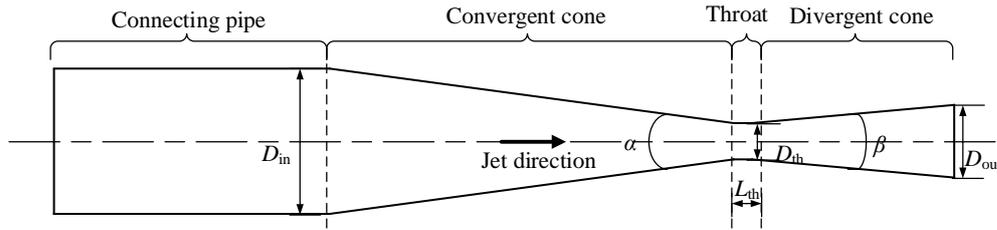
Fig. 2. Venture tube that is used as upstream nozzle.

Table 1 Specifications of the upstream nozzle

Inlet diameter D_{in}/mm	Exit diameter D_{out}/mm	Throat diameter D_{th}/mm	Throat length L_{th}/mm	Convergence angle $\alpha/°$	Diffusion angle $\beta/°$
8	4	2	1	16	10

assuming that the non-equilibrium phase transition effect and the heat transfer between the vapor and liquid phases were neglected, the transport equation of the liquid volume content is as follows:

$$\dot{m} = \frac{\partial \rho_1 \alpha_1}{\partial t} + \frac{\partial(\rho_1 \alpha_1 u_j)}{\partial x_j} = \dot{m}^+ + \dot{m}^- \qquad (6)$$

where the source term $\dot{m}^-$ represents the evaporation rate of the water in the flow field below the saturated vapor pressure, $\dot{m}^+$ indicates the condensation rate of the vapor in the flow field above the saturated vapor pressure.

The formula for calculating the rate of condensation $\dot{m}^+$ and the evaporation rate $\dot{m}^-$ is as follows:

$$m^+ = \frac{\rho_v \rho_l}{\rho_m} \alpha_v (1 - \alpha_v) \frac{3}{r_b} \left(\frac{2}{3} \frac{p_v - p}{\rho_l} \right)^{\frac{1}{2}} \quad (p \le p_v) \qquad (7)$$

$$m^- = \frac{\rho_v \rho_l}{\rho_m} \alpha_v (1 - \alpha_v) \frac{3}{r_b} \left(\frac{2}{3} \frac{p - p_v}{\rho_l} \right)^{\frac{1}{2}} \quad (p \ge p_v) \qquad (8)$$

Net mass source term is given by:

$$m^= - m^- = \frac{\rho_v \rho_l}{\rho_m} \frac{d\alpha_v}{dt} \qquad (9)$$

here α_v denotes volume fraction of vapor.

In the model, α_v is defined as:

$$\alpha_v = \frac{n_b \frac{4}{3} \pi R_b^3}{1 + n_b \frac{4}{3} \pi R_b^3} \qquad (10)$$

where n_b is bubble number density. R_b is the bubble radius which is expressed as:

$$R_b = \left(\frac{3\alpha_v}{4\pi(1 - \alpha_v)n_b} \right)^{1/3} \qquad (11)$$

2.2   Physical Model and Mesh Generation

Cavitation number is an important parameter to describe the degree of cavitation. The size of the hydraulic device has a strong influence on the cavitation number (Yan & Thorpe, 1990). Combined with predecessor research, a structure of venturi that

is more likely to generate cavitation and is used as the upstream nozzle of Helmholtz nozzle. In order to match the size of the oscillating cavity, the size of the venturi was correspondingly reduced. The final shape and dimensions of the upstream nozzle are shown in Fig. 2 and Table 1.

Rockwell concludes that the reason for the hydro-dynamically induced self-oscillation is the instability of the shear layer and the amplification of its unstable disturbance (Rochwell, 1983). Meanwhile, due to the existence of the collision boundary, the upstream of the shear layer is subjected to continuous unstable disturbance. The interaction between the collision wall of an angle of 90° and the jet minimal (Fang *et al.* 2012).

Therefore, collision angle of 90° is selected in order to highlight the variation of the oscillation characteristics due to replacing the upper part of a traditional contract structure with a venture tube one.

Structured mesh was employed to discrete the computational domain. For Helmholtz nozzle, pressure fluctuation and cavitation mainly occur at oscillating cavity. There are different situations for the composite nozzle, pressure fluctuations mainly occur in the oscillating cavity, but cavitation can be observed significantly in the upstream nozzle and oscillating cavity. Therefore, the meshes of the oscillating cavity and the upstream nozzle are refined. Grid independence tests were performed, and the grid size was increased by 25% each time until no noticeable variance in the velocity profile was observed. The grid case that Final selected for Helmholtz nozzle and Composite nozzle contained 5612744 and 5938716 nodes. The details of the meshing are shown in Fig. 3.
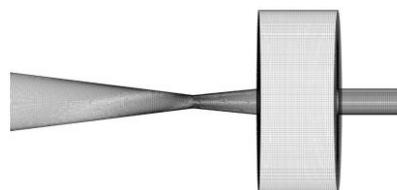

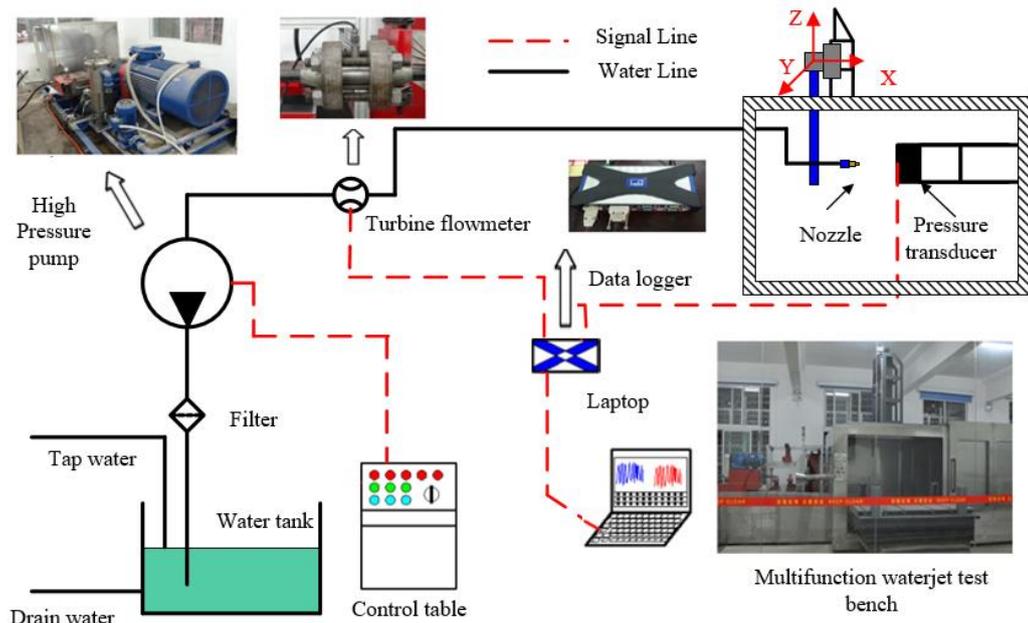**Fig. 3. Mesh generation of the Composite nozzle.**

Fig. 4. Experimental setup of the pressure test.

2.3 Numerical procedure

Before the transient calculation, the flow field obtained by the steady-state calculation was used as the initial field, and then the transient two-phase LES calculation was performed, which can shorten the time required for calculation. The near-wall area used the balanced stress model. The boundary conditions for both inlet and outlet were pressure boundary. The dispersion of the governing equations used the finite volume method. The time integral solution used the second-order implicit scheme. The convection term and the discrete term of the pressure term adopted the second-order upwind. Coupled scheme was adopted to solve the coupled equations of velocity and pressure. Due to the high Reynolds number of the jet field and the complicated flow in the Helmholtz oscillation cavity, the whole simulation time was 1 s in order to obtain the multiple oscillating periods and the time step was set as 10^{-5} s to capture the periodical variation of the two-phase flow instead of the real transient evolution of the cavitating flow.

The densities of pure water and vapor are 998.2kg/m³ and 0.02558kg/m³ respectively. The viscosity coefficient of pure water and vapor are 0.001kg/m·s and 1.26×10⁻⁶kg/m·s separately. The Vaporization pressure is p_v=3540Pa. The bubble radius is r_b=10⁻⁵m. Bubble number density is n_b=1.0×10¹³.

3 VALIDATIONS

3.1 Facilities and Experimental Setup

The experiment in order to verify the correctness of the algorithm is schematically shown in Fig. 4. The experiment was performed on a multifunction waterjet test bench, which was developed independently by our research group and had been applied in several previous investigations (Fang *et al.* 2014; Li *et al.* 2016).

The source of high pressure waterjet is a high-pressure piston pump with a flow rate of 120 L/min and a maximum pressure of 60MPa. The pump outlet was equipped with a turbine flowmeter to monitor its flow. And the pump pressure could be continuously regulated though a control table that could change the working frequency of the motor. The nozzle was mounted on a walking device that had X, Y, and Z motions with a precision of 0.1mm, shown in Fig. 4. As shown in the figure, a pressure sensor (Model: HELM91), which had been calibrated by the manufacture with an accuracy of ±0.5%FS, was installed on the target plate to get the pressure of inlet and outlet. During each test, both the average and real-time pressure could be directly read out from the laptop connected to the data logger (Model: HBM Quantum X MX840B-8), which had been calibrated by the manufacture with an accuracy of ±0.01%FS.

High pressure water impinged on the target plate in order to measure the pressures at nozzle outlet. Adjusting the position of the nozzle ensured that the distance between the nozzle and the target plate is 5mm. After the pressure of nozzle inlet stabilized at 5MPa, the data collected by the pressure transducer installed on the target plate was record.

The device and procedure of this experiment are simple. In order to eliminate the influence of pressure loss caused by the pipeline, a pressure sensor is placed at the nozzle inlet for measurement. Others, there was a NXQ capsule accumulator

connected to the pump to eliminate pressure fluctuations caused by unstable output of piston pump. Therefore, the uncertainty of the experiment mainly be determined by the pressure sensor used for pressure measurement and the data logger. Take the uncertainty propagation theory as the foundation, the equation for the total uncertainty of the experiment is as follows

$$E_t = \sqrt{E_s{}^2 + E_s{}^2 + E_l{}^2} \qquad (12)$$

where: E_s is the uncertainty of the pressure sensor; E_l is the uncertainty of the data logger.

The total uncertainty of the experimental system calculated according to the above formula is ±0.7%FS.

3.2 Comparison of Results

Comparison of the experimental and numerical simulation results between the composite nozzle and the conventional Helmholtz nozzle is showed in Fig. 5. The continuous 20 cycles of the pressure oscillation are separately counted based on experimental and simulation data. For the numerical results, the peak and average values of the pressure are 7.97MPa and 5.66MPa, while the experimental ones are 7.91MPa and 5.63MPa. The experimental values are smaller than the numerical ones and the error of pressure peak and average value are 0.7% and 0.6%, which is acceptable in the verification of numerical simulation.
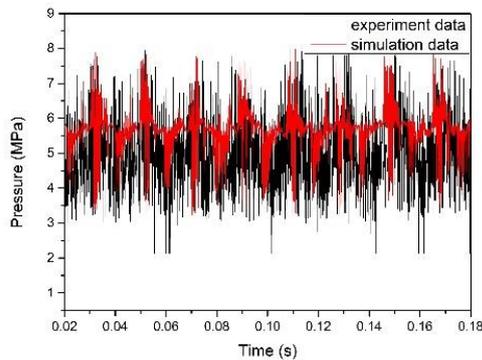

Fig. 5. Comparison of experiment and simulation.

In order to verify the results more accurately, the experimental and numerical results were processed by FFT method. The spectrum is presented in Fig. 6. There is a significant similarity in the pressure oscillation frequency domain diagram. The main frequencies captured in the experiment and simulation are 2340.01 Hz and 2362.78 Hz, respectively. The error is 0.9%, which is acceptable in the verification of numerical simulation.

4   RESULTS AND DISCUSSION

4.1 Vortex Structure in Cavity

The phenomenon of flow separation in the nozzle

can be visualized by the shedding of the vortex. Analyzing the vortex ring structure inside the whole nozzle contributes to the understanding of the flow characteristics in the cavity and the mechanism of its oscillation. In order to more clearly show the vortex characteristics, the Q criterion is used to identify the vortex (Jeong *et al.* 1995). The Q-criterion is defined as follows

$$Q = -\frac{1}{2}(S_{ij}S_{ij} - \Omega_{ij}\Omega_{ij}) \qquad (13)$$

Where

$$S_{ij} = \frac{1}{2}\left(\frac{\partial u_i}{\partial x_j} + \frac{\partial u_j}{\partial x_i}\right) = sym(\frac{\partial u_j}{\partial x_i}) \qquad (14)$$

$$\Omega_{ij} = \frac{1}{2}\left(\frac{\partial u_i}{\partial x_j} - \frac{\partial u_j}{\partial x_i}\right) = Asym(\frac{\partial u_i}{\partial x_j}) \qquad (15)$$

When the magnitude of the Q-criterion is positive, the positive regions are good indicators of turbulent structures.

Figure 7 shows the vortex (Iso-surface of Q=2.6×10⁷ s⁻²) in the two oscillation cavities at different times. This section mainly analyzes the effect of replacing the upper part of a traditional contract structure with a venture tube one on the entire injection process based on the evolution of vortex.
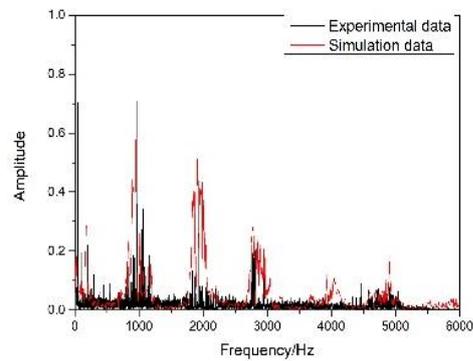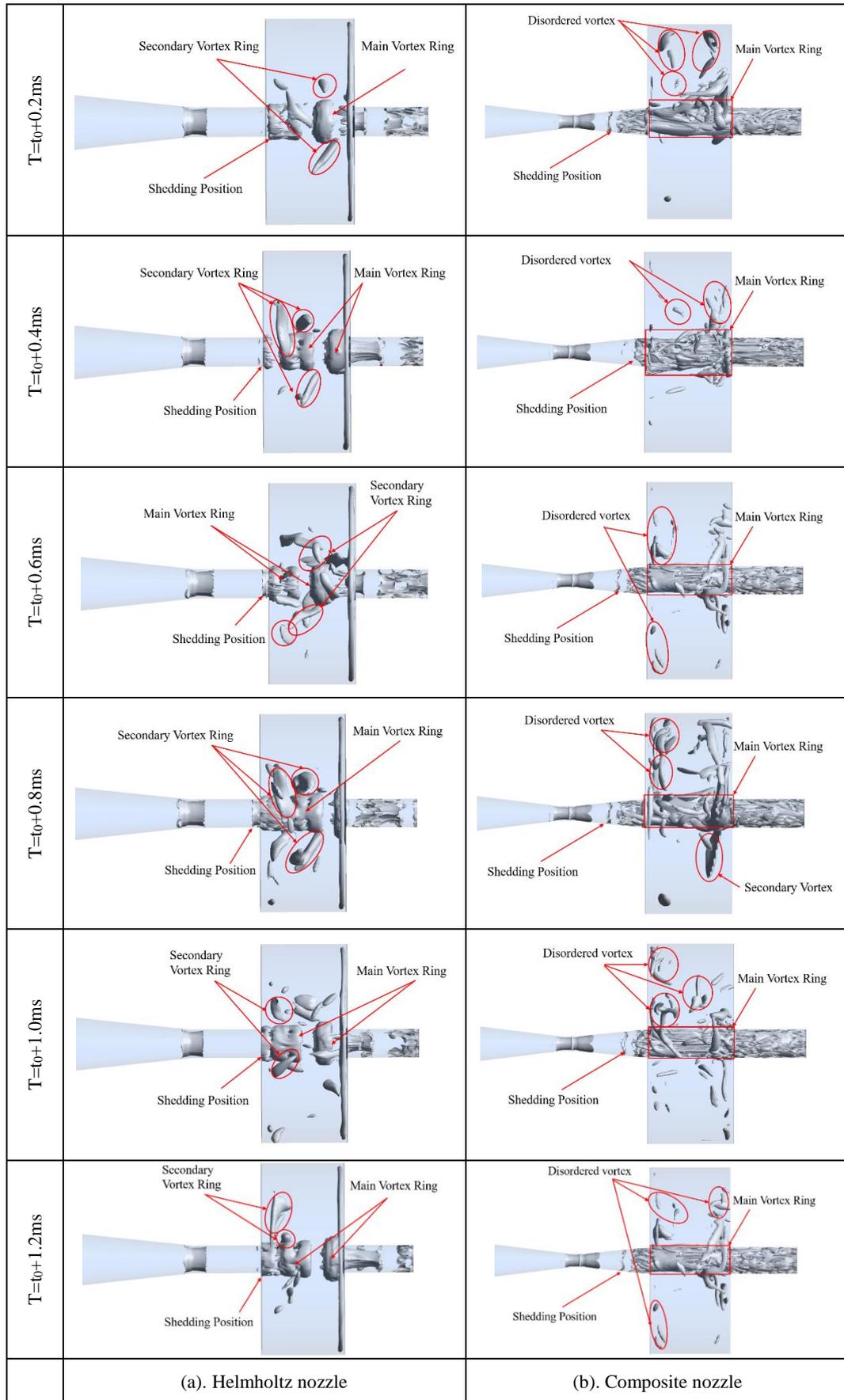

Fig. 6. Spectrum of pressure oscillation.

The evolution of the vortex ring inside the oscillating cavity is similar, although the structure of the upstream nozzle is different. The vortex ring is continuously enlarged and changed after shedding, and gradually loses stability. When approaching the downstream nozzle, the collision wall brings about the deformation of the main vortex ring. Subsequently, the main vortex impinges on the collision wall, breaking into small-scale vortices and gradually dissipating in the cavity.

Comparison of the vortex evolution process in the cavity of two nozzles, it is obvious that the shedding position of the main vortex ring moves forward. The main reason is that the separation of the boundary layer appears in the diffusion section of the upstream nozzle. The vortex formed during separation moves into the cavity with the main

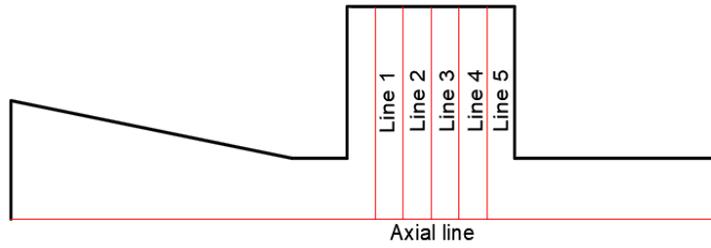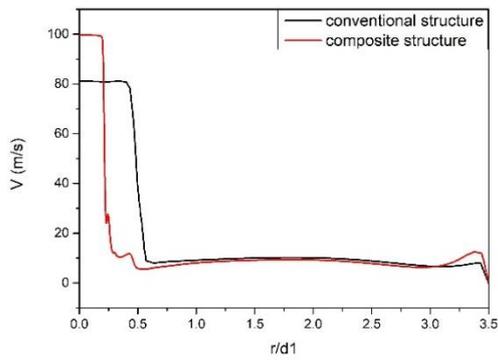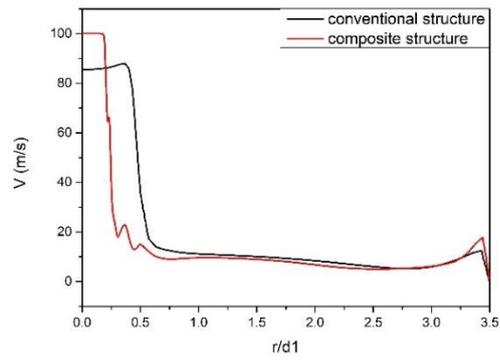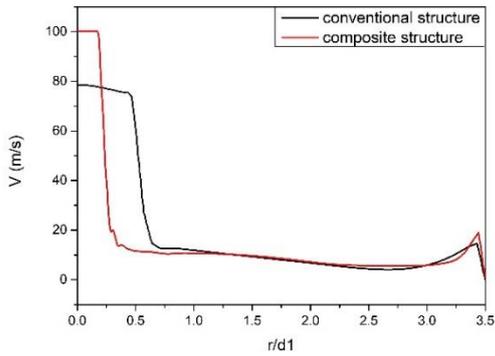**Fig. 7. Evolution process of vortex in oscillating cavity.**

(a). Helmholtz nozzle   (b). Composite nozzle

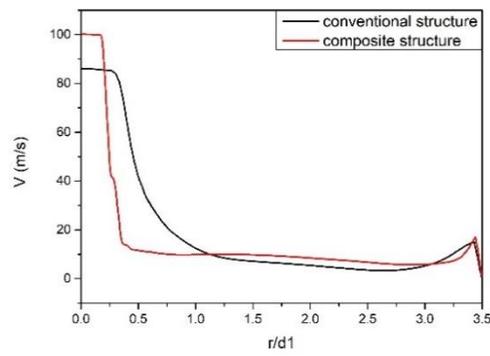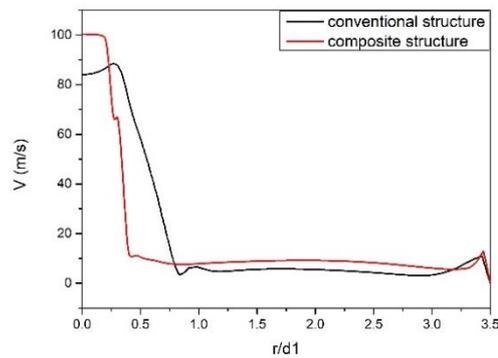**Fig. 8. Distribution of monitor lines.**

(a).Line 1

(b).Line 2

(c).Line 3

(d).Line 4

(e).Line 5

Fig. 9. Velocity distribution of different sections in the cavity.

flow. In addition, compared with the evolution process of the vortex ring in the cavity of the composite nozzle, the secondary vortex rings parallel with the main vortex ring in the radial direction can be clearly observed from Fig 7.a. Due to the addition of vortex rings, a large amount of energy is redistributed within the chamber, which reduces the energy output of the nozzle. Flow field in the cavity of the composite nozzle has obvious turbulent coherent structure. The disordered vortex generated by the interaction of the main vortex ring and the collision wall excites the oscillation of pressure near the edge of cavity. There is no secondary vortex ring in the chamber basically, which is beneficial to the reduction of energy dissipation. Therefore, the pressure oscillation near the edge of cavity becomes weak and the energy output of Composite nozzle increased, which is consistent with the results of Section 4.3.

4.2 Velocity Distribution in the Cavity

The jet enters the Helmholtz cavity after ejecting from the upstream nozzle. Due to the difference in velocity between the fluid and the edge, it is a typical shear flow. There is a strong momentum exchange between the fluids on both sides of the jet boundary. The velocity gradient in the flow field near the wall of cavity is very large. The monitoring lines are presented in Fig. 8.

Under the same boundary conditions, the velocity distributions on different sections in the cavity are respectively depicted and shown in Fig. 9. In Fig. 9, the $r/d1$ is the non-dimensional radial distance and the $d1$ is the radius of the oscillating cavity.

Obviously, the velocity distributions in the two structural cavities show the same trend. Since the flow velocity of the water entering the cavity is fast and the volume of the cavity is small, the axial velocity of the jet is substantially not attenuated.

However, the flow field in composite nozzle has a higher axial velocity, which is due to the constricted section in the upstream nozzle. The increase of velocity in the jet core caused by the change of nozzle structure means that a larger jet energy can be obtained at the nozzle outlet when the oscillation occurs. The constant velocity core of the flow field in the cavity is wider when using a conical nozzle as the upstream nozzle. Due to the more complicated vortex shedding at the upstream nozzle, significant changes of the flow field occurs at the jet shear layer. The change in the structure of the upstream nozzle makes the internal shearing of the jet shear layer more intense, which contributes to the enhancement of the pressure oscillation in the cavity.

4.3 The Characteristic of Pressure Oscillations

4.3.1 Pressure Oscillations in the Cavity

In order to further study the flow field characteristics

in the oscillating cavity, the XY plane of the figure is intercepted, and reference points are set at different positions in the upper cavity. Pressure oscillations at these points are monitored in order to analyze the frequency characteristics of the flow field. The distribution of the monitoring points is showed in Fig 10.

Figure 11 is a time-domain curve of pressure pulsation of each monitoring point at point 1 and point 2. At point 1, the amplitude of the pressure fluctuation is not large because the interference in the upstream inlet is small. Comparing the pressure fluctuations of point 1 for the two structures, the frequency of pressure fluctuations is higher in the composite nozzle. It should be noted that the instability of the shear layer is the fundamental cause of oscillation (Rockwell & Naudascher, 1979).

The change in the structure of the upstream nozzle, similar to the venturi, induces the high frequency shedding of the discrete vortex ring. Point 2 and point 1 are both on the nozzle axis. Due to the higher flow rate of the fluid near the axis, the effect of vortex ring and cavitation in the cavity is small, which results in a quiet change in the amplitude of the pressure oscillations at two points along the axis.
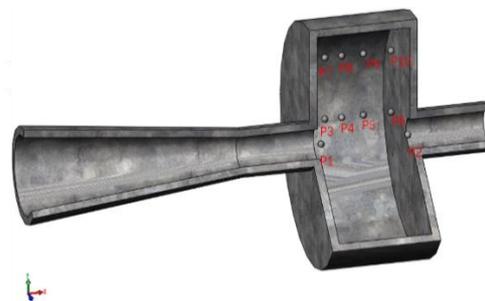

Fig. 10. Monitoring point located in the oscillating cavity.

The pressure fluctuations at point 3, 4, 5, and 6 in the oscillating cavity of two different structures are shown in Fig. 12. As can be seen in the figure, each point has a significant periodic pulsation and the amplitude of the oscillation increases gradually along the jet direction.

Fourier transform is operated for the pressure fluctuations at the various points, and the result is shown in Fig. 13. It is obvious that the amplitude of the pressure fluctuation is amplified along the direction of the jet. Comparing the pressure fluctuations at various points in the oscillation cavity of the two nozzles, it is obvious that the main frequency and the amplitude of pulses in the composite nozzle were higher. For point 3 located at the initial position of the vortex ring shedding,
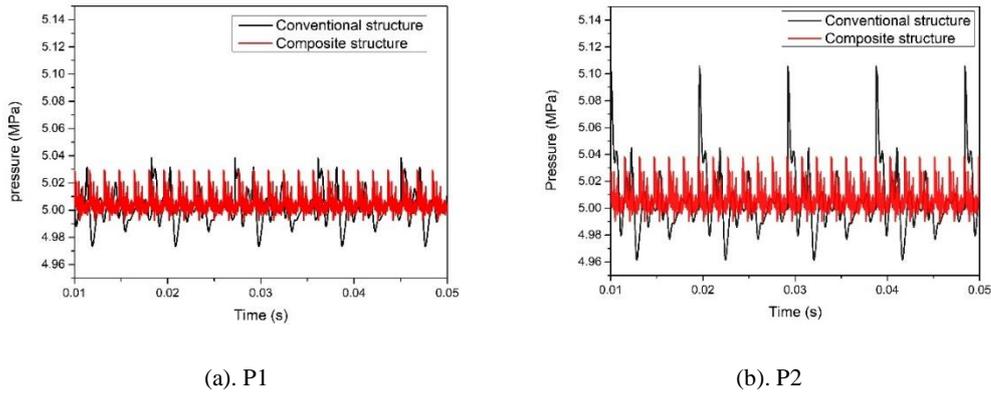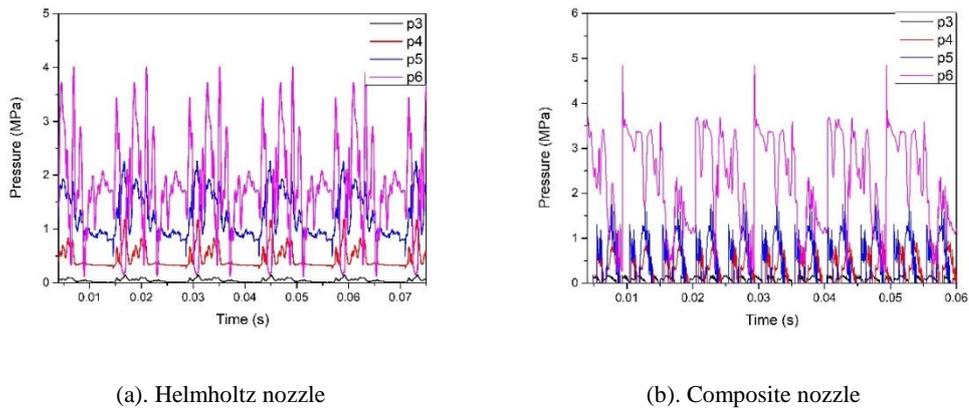
(a). P1   (b). P2

Fig. 11. Time domain of p1, p2.

(a). Helmholtz nozzle   (b). Composite nozzle

Fig. 12. Time domain of p3, p4, p5, p6.

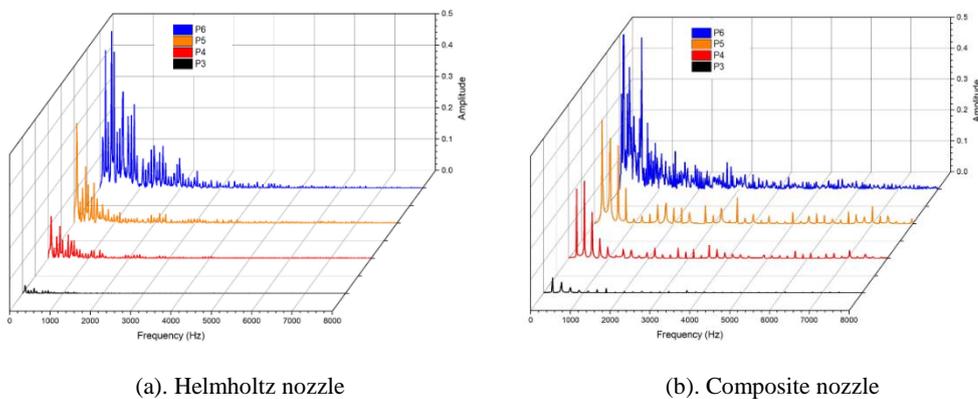(a). Helmholtz nozzle   (b). Composite nozzle

Fig. 13. Frequency domain of p3, p4, p5, p6.

although the pressure amplitude is not obvious from the time domain characteristic curve, the period of pressure oscillation is stable, and the main frequency is 227 Hz. The initial source of the disturbance amplification in the entire cavity is a stable low-frequency vortex shedding. The self-resonating oscillation jet is generated by the amplification of each stage. The main frequencies of point 4, 5, and 6 in the oscillation cavity of the composite nozzle are 390Hz, 406Hz and 552Hz, respectively. Since this area is close to the collision wall, the pulse around point 6 is affected by many factors such as the upstream vortex ring, the collapse of the bubble located near the collision wall, and the contraction of the downstream orifice. The frequency domain diagram of point 6 has multiple peaks, and the main frequency is not obvious.

The pressure fluctuations at point 7, 8, 9, and 10 in the oscillating cavity of two different structures are as shown in Fig. 14. There is a big difference
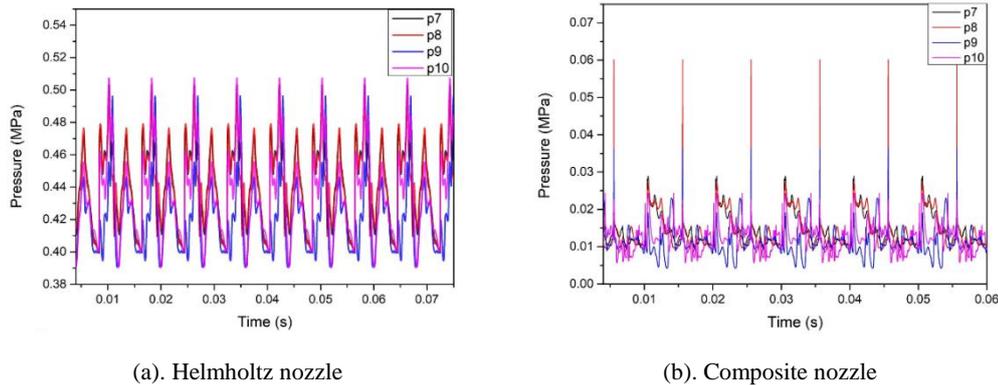
(a). Helmholtz nozzle   (b). Composite nozzle

Fig. 14. Time domain of p7, p8, p9, p10.

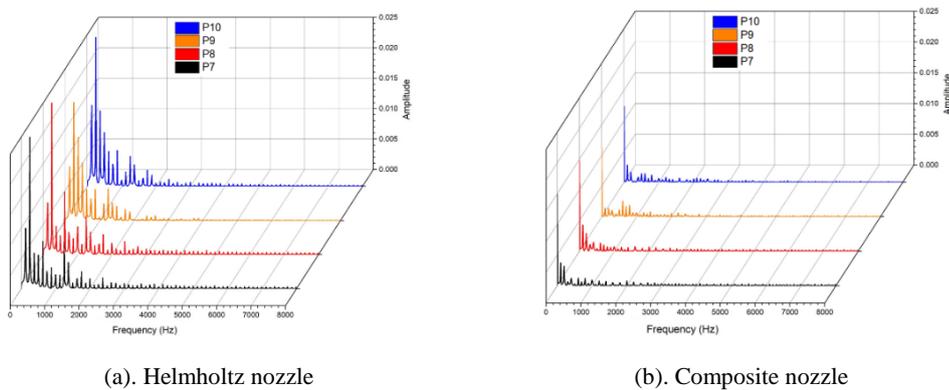(a). Helmholtz nozzle   (b). Composite nozzle

Fig. 15. Frequency domain of p7, p8, p9, p10.

between the pressure fluctuations of these points in the two structures. The instantaneous value of pressure is subtracted from the average value to obtain the pulsation value curve with time, and then subjected to FFT method to obtain the amplitude frequency information of the pressure pulsation of each pressure measuring point, as shown in Fig. 15. The edge of the cavity is less affected by the jet axis and can only produce stable pulsations with small frequencies and amplitudes.

In summary, there are significant differences in the amplitude and frequency characteristics of the pressure oscillations at various points for the two nozzles, which is in consistent with the evolution of the vortex ring in the cavity. Since these points are located at the edge of the cavity, secondary vortex rings are difficult to affect the pressure oscillations at these positions.

The pressure oscillation frequency of the two points on the nozzle axis is obviously improved. So there is no doubt that the shedding frequency of the vortex ring at the upstream nozzle increases for the Composite nozzle. The pressure oscillation of point 3, 4, 5, and 6 in the composite nozzle is more intense, which is related to the evolution process of vortex. The frequency of the pressure oscillation is

controlled by the vortex shedding frequency. On the one hand, the energy dissipation in the cavity reduced with the decrease of the secondary vortex ring, which makes the amplitude of pressure oscillation increasing. On the other hand, for these points near the edge of cavity, secondary vortex ring induces the oscillation of pressure [18]. Therefore, the pressure oscillation at this position becomes weak.

4.3.2 Pressure Oscillation at the Outlet of Nozzle

The ultimate goal of studying the mechanism of self-resonating jet and changing the structure of Helmholtz nozzle is to improve the performance of self-resonating jet, which is mainly reflected in the pressure oscillation at the nozzle outlet.

Table 2 shows the main parameters of pressure oscillation in nozzle outlet, which is obtained by numerical simulation. As can be seen from the table, the structural change of upstream nozzle results in the improvement of self-resonating jet performance. After the change of nozzle structure, the main frequency of the pressure oscillation in the nozzle outlet rises to 2362.78Hz and the peak and average values of pressure in the nozzle outlet respectively increased by 45% and 12.5%.

Table 2 Main parameters of pressure oscillation in nozzle outlet

	Peak of pressure oscillation/MPa	Average value of pressure oscillation/MPa	Main frequency of pressure oscillation/Hz
Helmholtz nozzle	5.49	5.03	956.37
Composite nozzle	7.97	5.66	2362.78

5. CONCLUSION

In this paper, the influence of the upstream nozzle structure on the performance of the self-resonating jet is studied by numerical method, and the results are verified experimentally. The main conclusions of the study are shown as follows:

(1) The structural change of upstream nozzle results in the improvement of self-resonating jet performance. The main frequency of the pressure oscillation in the nozzle outlet rises to 2362.78Hz. Others, the peak and average values of pressure in the nozzle outlet respectively increased by 45% and 12.5%.

(2) The convergence-diffusion structure in the upstream nozzle makes the shedding position of the main vortex ring moving forward and increases the shedding frequency of vortex, which causes massive reductions of the secondary vortex ring in the chamber, even vanishes.

(3) For the Composite nozzle, the constant velocity core in the chamber becomes smaller and has a higher axial velocity, which means that a larger jet energy can be obtained at the nozzle outlet when the oscillation occurs.

(4) After the change of nozzle structure, the pressure oscillation in the central region of the oscillating chamber becomes stronger. On the contrary, the pressure oscillation in the edge region of the chamber subsides. This phenomenon is consistent with the change of Vortex structure in cavity.

For self-oscillating jets, the size of the oscillating cavity has a significant effect on jet characteristics. We have not changed the size of the chamber in this simulation due to the huge number of grids. Therefore, this preliminary study only does provide qualitative-only results and more accurate modulation should be achieved in future studies by considering the size of the chamber.

ACKNOWLEDGEMENTS

REFERENCES

Annoni, M., L. Cristaldi, M. Norgia, and C. Svelto, (2008). Measurement of water jet velocity distribution using laser velocimetry. *IEEE Transactions on Instrumentation and Measurement* 57(8), 1524-1528.

Barre, S., J. Rolland, G. Boitel, E. Goncalves, and R. F. Patella (2009). Experiments and modeling of cavitating flows in venturi: attached sheet cavitation. *European Journal of Mechanics* 28 (3), 444-464.

Chahine, G. L. and V. E. Johnson (1985). Mechanics and applications of self-resonating cavitating jets. *International Symposium on Jets & Cavities, Asme, Wam,* 271–284.

Chen, G., G. Wang, C. Hu, B. Huang, Y. Gao, and M. Zhang (2015). Combined experimental and computational investigation of cavitation evolution and excited pressure fluctuation in a convergent–divergent channel. *International Journal of Multiphase Flow* 72, 133-140.

Chen, H., H. Yi, K. Yong (2019). Fracture initiation and propagation under different perforation orientation angles in supercritical CO2 fracturing. *Journal of Petroleum Science and Engineering* 183, 106403.

Dehkhoda, S. and M. Hood (2013). An experimental study of surface and sub-surface damage in pulsed water-jet breakage of rocks. *International Journal of Rock Mechanics and Mining Sciences* 63, 138-147.

Dehkhoda, S. and M. Hood (2014). The internal failure of rock samples subjected to pulsed water jet impacts. *International Journal of Rock Mechanics and Mining Sciences* 66, 91-96.

Fang, Z. L., Y. Kang, X. F. Yang, B. Yuan, and D. Li (2012). The influence of collapse wall on self-excited oscillation pulsed jet nozzle performance. *IOP Conference Series Earth and Environmental Science* 15(5), 2022.

Fang, Z. L. , Y. Kang, X. C. Wang, D. Li, and X. Y. Wang(2014). Numerical and experimental investigation on flow field characteristics of organ pipe nozzle. *IOP Conference Series Earth and Environmental Science*, 22(5), 052020.

Germano, M., U. Piomelli, P. Moin, and W. H. Cabot (1991). A dynamic subgrid-scale eddy

viscosity model. *Physics of Fluids A* 3(3), 1760-1765.

Geveci, M., P. Oshkai, D. Rockwell, J. C. Lin, and M. Pollack (2004). Imaging of the self-excited oscillation of flow past a cavity during generation of a flow tone. *Journal of Fluids & Structures* 18(6), 665-694.

Gould, K., S. Q. Cai, C. Neft and A. Bhunia (2015). Liquid jet impingement cooling of a silicon carbide power conversion module for vehicle applications. *IEEE Transactions on Power Electronics* 30(6), 2975-2984.

Hsu, C. Y., C. C. Liang, T. L. Teng and A. T. Nguyen (2013). A numerical study on high-speed water jet impact. *Ocean Engineering* 72, 98-106.

Hu, Y., Y. Kang and X. C. Wang (2014). Mechanism and experimental investigation of ultra high pressure water jet on rubber cutting. *International Journal of Precision Engineering and Manufacturing* 15(9), 1973-1978.

Ishfaq, K., N. A. Mufti, N. Ahmed, and S. Pervaiz (2018). Abrasive waterjet cutting of cladded material: kerf taper and mrr analysis. *Materials and Manufacturing Processes* (3), 1-10.

Jeong, J. J. J. and F. Hussain (1995). On the identification of a vortex. *Journal of Fluid Mechanics* 332(1), 339-363.

Johnson, V. E. J., W. T. Lindenmuth, A. F. Conn and G. S. Frederick (1981). Feasibility study of tuned-resonator, pulsating cavitating water jet for deep-hole drilling. *Petroleum*.

Kolšek, T., Jelić, Nikola, Duhovnik, Jože (2007). Numerical study of flow asymmetry and self-sustained jet oscillations in geometrically symmetric cavities. *Applied Mathematical Modelling* 31(10), 2355-2373.

Kuo, C. H., S. H. Huang, and C. W. Chang (2000). Self-sustained oscillation induced by horizontal cover plate above cavity. *Journal of Fluids & Structures* 14(1), 25-48.

Li, D., Y. Kang, X. Wang, X. Ding, and Z. Fang (2016). Effects of nozzle inner surface roughness on the cavitation erosion characteristics of high speed submerged jets. *Experimental Thermal and Fluid Science* 74, 444-452.

Li., G., S. Zhonghou, Z. Changshan, Z. Debin, and C. Hongbing (2005). Investigation and application of self-resonating cavitating water jet in petroleum engineering. *Petroleum Science and Technology* 23(1), 1-15.

Liao, Z., J. Li, D. Chen, X. Deng, and F. Zhang (2003). Theory and experimental study of the self-excited oscillation pulsed jet nozzle. *Chinese Journal of Mechanical Engineering* 16(4), 379-383.

Lilly, D. K (1992). A proposed modification of the germano subgrid-scale closure method. *Physics of Fluids* A, 4.

Liu, W., Y. Kang, M. Zhang, X. Wang, D. Li, and L. Xie (2018). Experimental and theoretical analysis on chamber pressure of a self-resonating cavitation waterjet. *Ocean Engineering* 151, 33-45.

Lu, Y., F. Huang, X. Liu, and X. Ao (2015). On the failure pattern of sandstone impacted by high-velocity water jet. *International Journal of Impact Engineering* 76, 67-74.

Meganathan, A. and A. Vakili (2002). An experimental study of open cavity flows at low subsonic speeds. *AIAA*, 2002-0280.

Morel, T. (1979). Experimental study of a jet-driven helmholtz oscillator. *Journal of Fluids Engineering* 101(3), 383.

Rockwell, D. (1983). Oscillations of impinging shear layers. *AIAA Journal* 21(5), 645-664.

Rockwell, D. and E. Naudascher(1979). Self-sustained oscillations of impinging free shear layers. *Annual Review of Fluid Mechanics* 11(1), 67-94.

Rockwell, D., J. C. Lin, P. Oshkai, M. Reiss, and M. L. Pollack (2003). Shallow cavity flow tone experiments: onset of locked on states. *Journal of Fluids & Structures* 17(3), 381-414.

Sato, K., K. Hachino, and Y. Saito (2003). Inception and Dynamics of Traveling-Bubble-Type Cavitation in a Venturi. *Asme/jsme Joint Fluids Summer Engineering Conference*.

Soyama, H (2013). Effect of nozzle geometry on a standard cavitation erosion test using a cavitating jet. *Wear* 297(1-2), 895-902.

Stutz, B and J. L. Reboud (2000). Measurements within unsteady cavitation. *Experiments in Fluids* 29(6), 545-552.

Yan, Y. and R. B. Thorpe (1990). Flow regime transitions due to cavitation in the flow through an orifice. *International Journal of Multiphase Flow* 16(6), 1023-1045.

Yazici, B., I. H. Tuncer, and M. A. Ak (2007). Numerical & Experimental Investigation of Flow Through A Cavitating Venturi. *International Conference on Recent Advances in Space Technologies. IEEE*.

Yuan, W., J. Sauer and G. H. Schnerr (2001). Modeling and computation of unsteady cavitation flows in injection nozzles. *Mécanique & Industries* 2(5), 383-394.

Zelenak, M., J. Foldyna, J. Scucka, S. Hloch, and Z. Riha (2015). Visualisation and measurement of high-speed pulsating and continuous water jets. *Measurement* 72, 1-8.